Int J Earth Sci (Geol Rundsch) (2017) 106:1107–1121
DOI 10.1007/s00531-016-1357-5

ORIGINAL PAPER

Mafic monogenetic vents at the Descabezado Grande volcanic field (35.5°S–70.8°W): the northernmost evidence of regional primitive volcanism in the Southern Volcanic Zone of Chile

Pablo A. Salas[1] · Osvaldo M. Rabbia[2] · Laura B. Hernández[2] · Philipp Ruprecht[3]

Received: 5 December 2015 / Accepted: 13 June 2016 / Published online: 27 June 2016

Abstract In the Andean Southern Volcanic Zone (SVZ), the broad distribution of mafic compositions along the recent volcanic arc occurs mainly south of 37°S, above a comparatively thin continental crust (≤~35 km) and mostly associated with the dextral strike-slip regime of the Liquiñe–Ofqui Fault Zone (LOFZ). North of 36°S, mafic compositions are scarce. This would be in part related to the effect resulting from protracted periods of trapping of less evolved ascending magmas beneath a thick Meso-Cenozoic volcano-sedimentary cover that lead to more evolved compositions in volcanic rocks erupted at the surface. Here, we present whole-rock and olivine mineral chemistry data for mafic rocks from four monogenetic vents developed above a SVZ segment of thick crust (~45 km) in the Descabezado Grande volcanic field (~35.5°S). Whole-rock chemistry (MgO > 8 wt%) and compositional variations in olivine (92 ≥ Fo ≥ 88 and Ni up to ~3650 ppm) indicate that some of the basaltic products erupted through these vents (e.g., Los Hornitos monogenetic cones) represent primitive arc magmas reaching high crustal levels. The combined use of satellite images, regional data analysis and field observations allow to recognize at least 38 mafic monogenetic volcanoes dispersed over an area of about 5000 km^2 between 35.5° and 36.5°S. A link between ancient structures inherited from pre-Andean tectonics and the emplacement and distribution of this mafic volcanism is suggested as a first-order structural control that may explain the widespread occurrence of mafic volcanism in this Andean arc segment with thick crust.

Keywords Monogenetic volcanism · Andean Southern Volcanic Zone · Descabezado Grande volcanic field · Olivine

Introduction

Mafic monogenetic volcanoes comprise edifices with a small cumulative volume (typically ≤1 km^3) that have been built up by one continuous, or many discontinuous, small eruptions that occurred over a brief time interval, often with different eruption styles, from highly explosive to effusive regimes leading to different landforms, such as spatter and pyroclastic cones, maar-diatremes and tuff rings (e.g., Németh and Kereszturi 2015; Johnson et al. 2008; Roberge et al. 2015; Genareau et al. 2010; Valentine and Gregg 2008). A common feature of monogenetic volcanoes is the primitive nature of the erupted products, suggesting that they represent the composition of deep-seated magmas that are able to traverse the crust in short timescales with minimal cooling (e.g., Ruprecht and Plank 2013), thereby minimizing compositional evolution by shallow crystallization, thus providing key insights into how the mantle produces its partial melts and how that melt rise to the surface (Németh and Kereszturi 2015). Conversely, long-term differentiation processes commonly associated with stratovolcanoes accounts for modifications of primary magmatic

Electronic supplementary material The online version of this article (doi:10.1007/s00531-016-1357-5) contains supplementary material, which is available to authorized users.

✉ Osvaldo M. Rabbia
rabbia@udec.cl

[1] Departamento de Ciencias de la Tierra, Universidad de Concepción, Casilla 160 C, Concepción, Chile

[2] Instituto de Geología Económica Aplicada GEA, Universidad de Concepción, Casilla 160 C, Concepción, Chile

[3] Lamont-Doherty Earth Observatory of Columbia University, 61 Route 9W, Palisades, NY 10964, USA

compositions, as evidenced by the scarcity of primitive, non-cumulate, high-MgO (>8 wt%) magmas potentially in equilibrium with the mantle wedge in volcanic arc suites (Hildreth and Moorbath 1988; Annen et al. 2006).

Recent magmatism in the Andean SVZ results from subduction of the Nazca Plate beneath South America at a trench normal convergence velocity of ~40 mm/year (e.g., Maloney, et al. 2013). This belt includes volcanoes from the marginal portion of the Pampean flat slab segment at 33°S to the latitude of the subduction of Chile Ridge at 46°S. The Andean SVZ has been divided into several segments based on petrographic, geochemical and isotopic variations of erupted rocks, spatial volcano distribution and incoming fracture zones (e.g., Völker et al. 2011; Dungan et al. 2001; Hildreth and Moorbath 1988; López-Escobar et al. 1995). According to López-Escobar et al. (1995), four distinctive segments or provinces are recognized in the current arc: northern (NSVZ, 33°–34.5°S), transitional (TSVZ, 34.5°–37°S), central (CSVZ, 37°–41.5°S) and southern (SSVZ, 41.5°–46°S). Compositional variations of erupted magmas indicate a higher basalt/rhyolite ratio in the CSVZ and SSVZ compared with the NSVZ and TSVZ segments. In addition, andesite and dacite are the dominant rock types erupted in the NSVZ and TSVZ (Stern 2004).

Crustal thickness beneath the SVZ decreases toward the south, from ~50 km in the NSVZ, ~45 km in the southern part of TSVZ (~36°S) and ~30 km thick at the southern end of the SSVZ (Tassara and Echaurren 2012).

The distribution of mafic monogenetic volcanoes in the SVZ is mostly restricted to its southern portion (south of ~38°S) in the CSVZ and SSVZ segments (e.g., López-Escobar et al. 1995), where the continental crust is thinner than ~35 km (e.g., Tassara and Echaurren 2012). Here, this mafic volcanism is structurally related to the main NNE-trending lineaments of the Liquiñe–Ofqui Fault Zone (LOFZ) and/or contained in a subsidiary trend oriented ENE, as it is the case for the Carrán–Los Venados mafic volcanic group (López-Escobar et al. 1995; Bucchi et al. 2015; Morgado et al. 2015). North of 38°S in a thicker crust environment, mafic monogenetic volcanoes are scarce. Moreover, any basaltic product (lava or pyroclastic deposit) becomes uncommon northward of 36°S, and true basalts (<52 wt% of SiO_2) are not reported north of this latitude. The most mafic lavas (~52 wt% of SiO_2) from the Planchón–Peteroa volcano (~35.3°S at the TSVZ; PPV in Fig. 1b) may represent the northernmost appearance of volcanic products with near-basaltic compositions throughout the entire volcanic belt. Southward, in the TSVZ at about 36°S, mafic products are present in minor proportions at the Tatara–San Pedro volcanic complex (e.g., Dungan et al. 2001; Fig. 2) and also at Nevado de Longaví volcano (Sellés et al. 2004; Rodríguez et al. 2007; Fig. 2), located ~36 km toward the southwest of the former volcanic complex (Figs. 1b, 2).

Fig. 1 **a** Location of the Andean Southern Volcanic Zone (SVZ) in the context of South America. The segmentation along the arc is shown in the *right inset* (López-Escobar et al. 1995). **b** Distribution of main volcanic centers in the Transitional SVZ. From north to south corresponds to the following volcanoes: Tinguiririca (TGV), Planchón–Peteroa (PPV), Descabezado Grande (DGV), Quizapu (QZV), Azul (AZV), Tatara–San Pedro (TSV), Pellado (PEV), Nevado de Longaví (NLV) and Chillán (CHV). *Segmented area* corresponds to enlarged area in **c**. **c** Distribution of mafic monogenetic volcanoes in the segment between 35.5° and 36.5°S. Segmented area shows the location of minor vents in the Descabezado Grande volcanic field (DGVF), and those are La Resolana craters (LRC), Los Hornitos cones (LHC) and older volcanism of Manantial Pelado cones (MPC) and Las Casitas volcanic field (CAS). Puelche (PVF) and Laguna del Maule (LdM) volcanic fields are also *highlighted*. Spatial distribution of NNW–SSE and NE–SW lineaments and vents is shown. A detailed classification of groups is given in Table 1

In this contribution, we address the conspicuous presence of a dispersed mafic monogenetic volcanic field occurring along a 100-km segment in the TSVZ, between 35.5° and 36.5°S, where crustal thickness reaches up to above 45 km (e.g., Tassara and Echaurren 2012). Petrography, whole-rock and olivine mineral chemistry data from Los Hornitos cones (LHC) and La Resolana craters (LRC), at the southwest flank of Descabezado Grande volcanic field (Maule Region, Fig. 1c), are used to support the presence of near-primary basalts in the TSVZ. Results are then discussed in a regional context using published information, and implications for the current distribution and long-term record of mafic volcanic products in the area are also provided.

Distribution of recent mafic monogenetic volcanoes in the TSVZ between 35.5° and 36.5°S

Los Hornitos cones, located 11 km southwest of Quizapu crater (Figs. 1c, 3, 4), consist of two twinned pyroclastic cones constituted by pyroclastic fallout deposits, scoria cones and associated lava flows (Fig. 5a, b). The two cones are named LHC-West and East, referring to their spatial relation. High-forsterite (Fo) olivine compositions (up to Fo_{91}) hosting sulfur-rich (up to ~3000 ppm) melt inclusions have been reported from Los Hornitos (Salas et al. 2009, 2014, 2015; Wehrmann et al. 2014), reflecting the participation of primitive magmas and the prevalence of near-undegassed conditions during the trapping of melts.

Aside from composition, an obvious difference between Los Hornitos and La Resolana craters, located 8 km apart from each other, is their different eruptive character. LRC represent a cluster of three maar-like vents, here referred to as LRC-North, Central and South. In addition to tephra deposits, lava erupted at LRC-North while only tephra

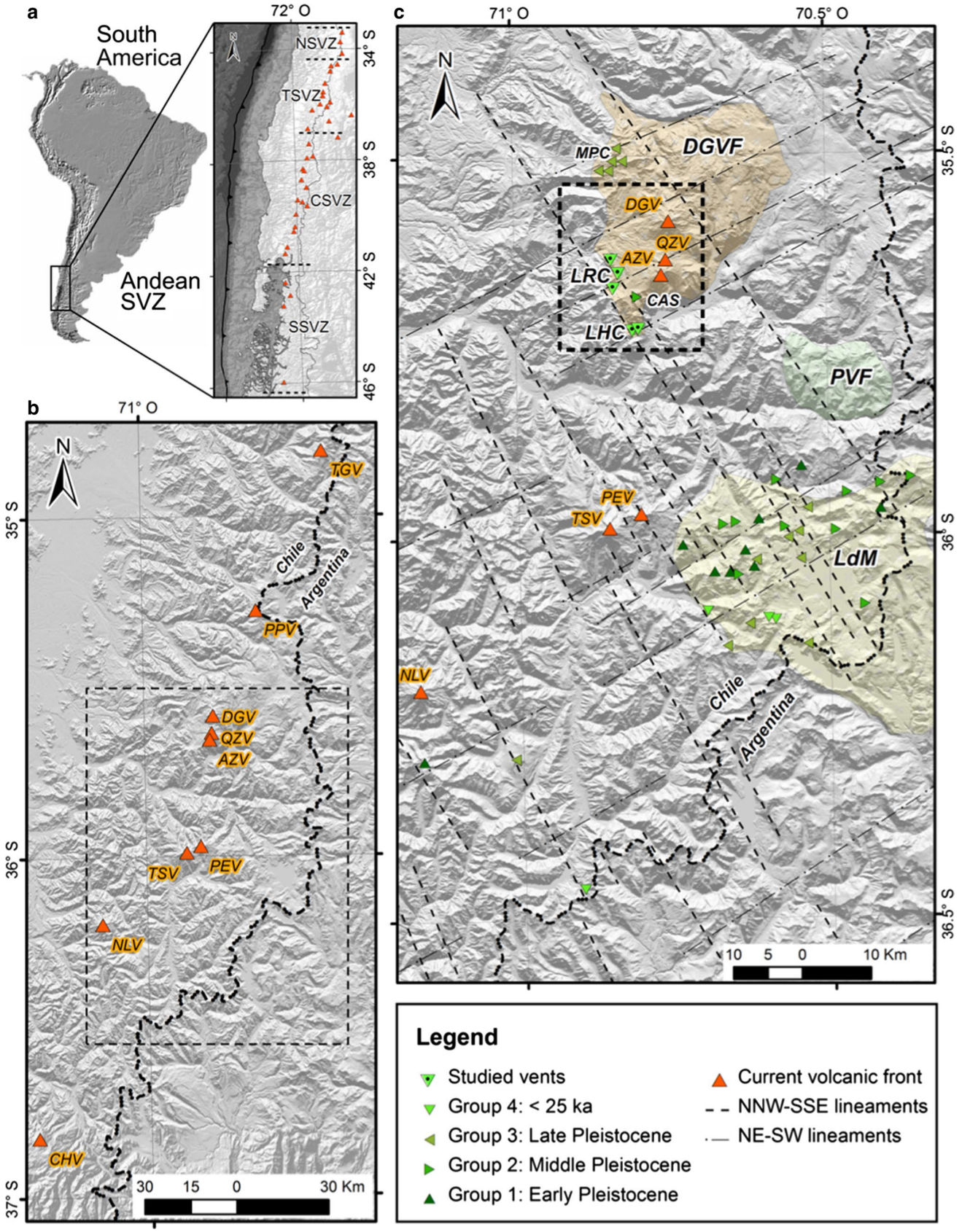
a
South America
Andean SVZ
72° O
34° S
38° S
42° S
46° S
NSVZ
TSVZ
CSVZ
SSVZ
b
71° O
35° S
36° S
37° S
N
TGV
Chile
Argentina
PPV
DGV
QZV
AZV
TSV
PEV
NLV
CHV
30 15 0 30 Km
c
71° O
70.5° O
35.5° S
36° S
36.5° S
N
MPC
DGVF
DGV
QZV
AZV
LRC
CAS
LHC
PVF
PEV
TSV
LdM
NLV
Chile
Argentina
10 5 0 10 Km
Legend
Studied vents
Group 4: < 25 ka
Group 3: Late Pleistocene
Group 2: Middle Pleistocene
Group 1: Early Pleistocene
Current volcanic front
NNW-SSE lineaments
NE-SW lineaments

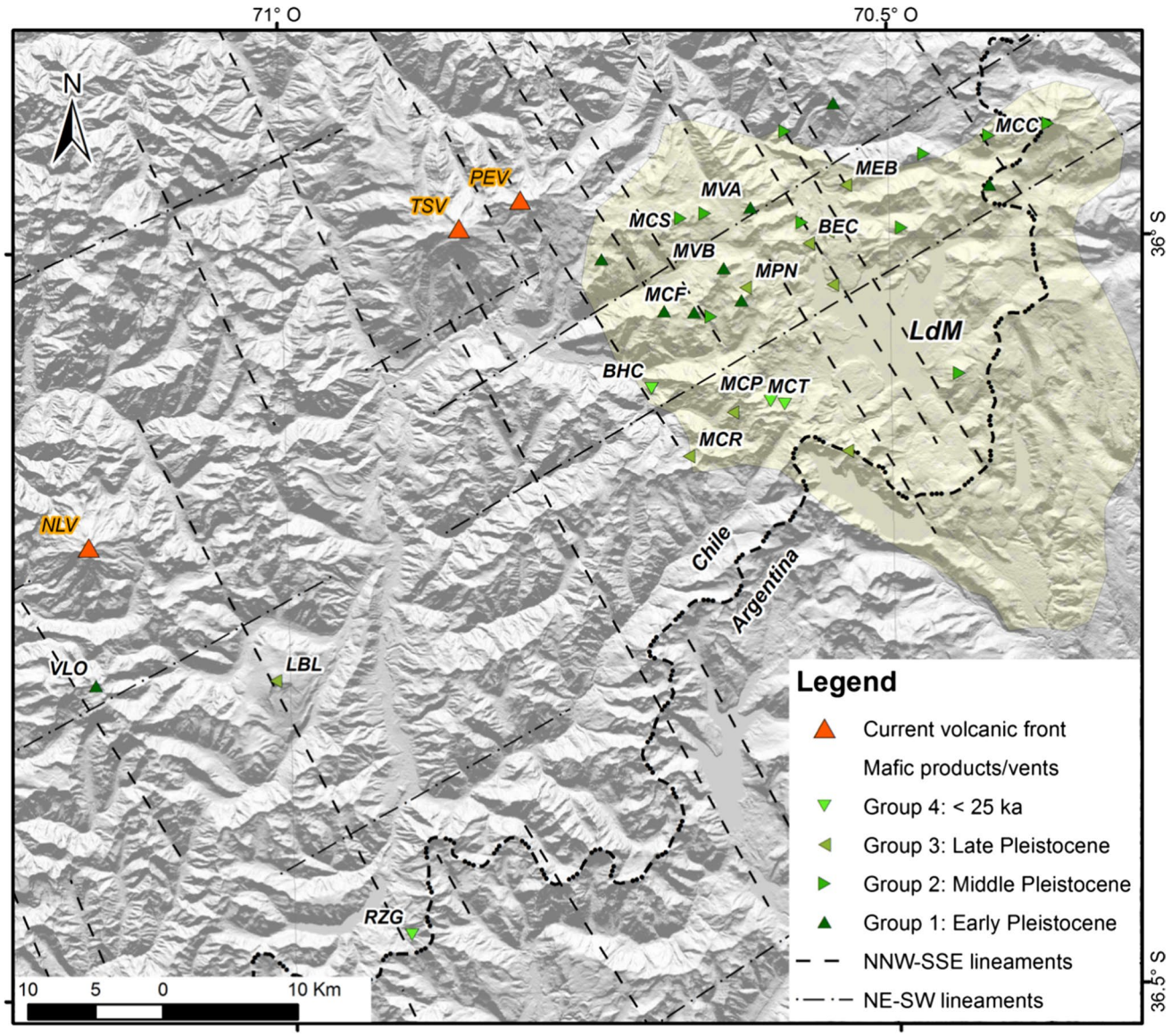

Fig. 2 Distribution of monogenetic mafic volcanoes in the Laguna del Maule volcanic field (LdM) and the three isolated vents of Loma Blanca (LBL), Rezago (RZG) and Villalobos (VLO) to the southern border. A detailed classification of groups is given in Table 1

deposits are found associated with LRC-Central and South craters (Fig. 5c).

Approximately 50 km southeast of the study area, at least three post-glacial (<25 ka) mafic units (basalt and mafic andesites) are present in the Laguna del Maule volcanic field (LdM; Fig. 2) (Hildreth et al. 2010). These include the pyroclastic cone and associated lava flows of Hoyo Colorado basalt (BHC), the andesite of Arroyo Cabeceras de Troncoso (MCT) and Crater 2657 andesite (MCP). Additionally, eight silicic andesite units are recognized in this volcanic field (not shown in Fig. 2). The Rezago volcano (RZG) is another scoria cone with associated tephra deposits and lava flows located in the southern end of the TSVZ segment at about 40 km south of LdM (Fig. 2).

Considering the preservation state of volcanic products, the five vents (LRC-North, Central, South and LHC-West and East) located in the Descabezado Grande volcanic field (DGVF) together with BHC and RZG appear to be more recent than MCT and MCP, although their precise ages have not been determined yet.

Monogenetic cones from the DGVF are located at 7.5 km west of the Quizapu volcano, a young and voluminous vent which erupted ~10 km^3 of andesite to dacite magmas in two eruptive events separated by 86 years (Hildreth and Drake 1992; Ruprecht et al. 2012; Higgins et al. 2015). The participation of mafic magma is documented in both eruptive episodes: as microgranular mafic enclaves during the effusive event of 1846–1847 and as mafic scoria emission during

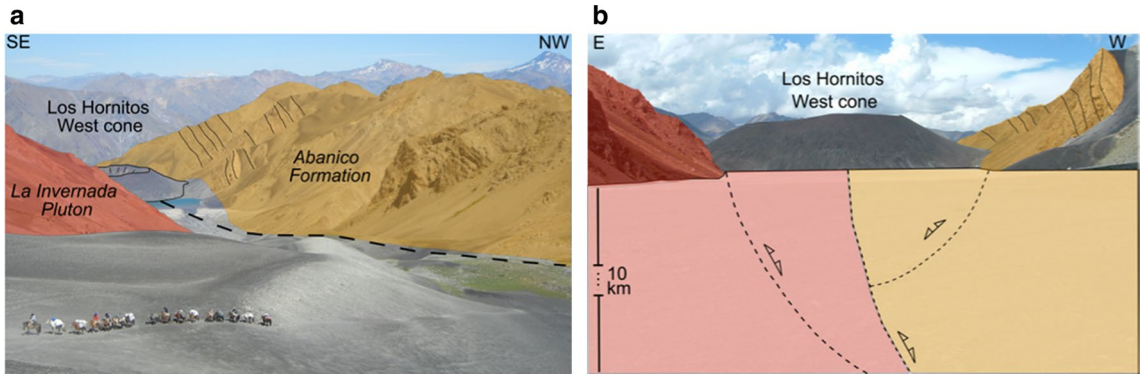

Fig. 3 **a** Panoramic view looking southward to Los Hornitos valley, showing the position of the cone just on the contact between the folded Abanico Formation and La Invernada Pluton. *Segmented line* is showing the trace of an inferred fault system along the NNW valley. **b** Conceptual model based in Astaburuaga (2014) representing a schematic motion of blocks during the extensional and contractional Cenozoic events. Note that this structural environment is coherent with the inversion of normal faults that compartmentalized the extensional Abanico Basin during the Mio-Pliocene compressive event (Piquer et al. 2015; Astaburuaga 2014)

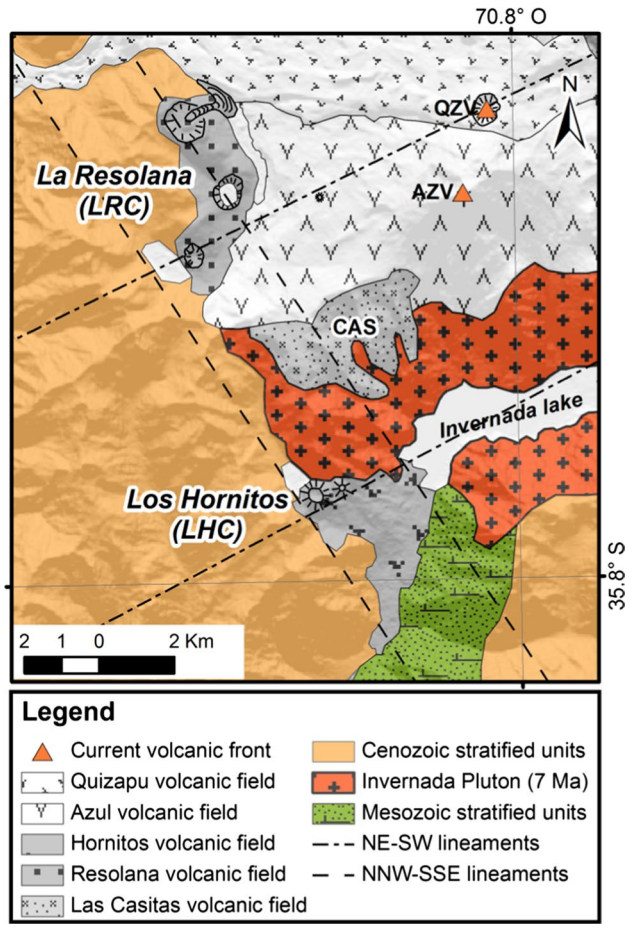

Fig. 4 Geological map of the surrounding area of Los Hornitos (LHC) and La Resolana (LRC) vents. Regional NNW–SSE and NE–SW lineaments are shown. The age of La Invernada pluton is taken from Hildreth and Drake (1992)

initial and terminal stages of the plinian event of 1932 (Hildreth and Drake 1992; Salas et al. 2009; Ruprecht et al. 2012). Considering the young character (<25 ka) of LRC and LHC and the historical eruptions of Quizapu volcano, below we compare a whole-rock geochemical and olivine mineral chemistry between these mafic products to discuss how their crustal transit may have varied.

Regional tectonic features in the area of Descabezado Grande volcanic field

At regional scale, the mafic vents occurring in the western edge of DGVF, including Los Hornitos cones and La Resolana craters, are located in the boundary between two basement domains, the Mesozoic (to the east) and the Cenozoic (to the west). In the study area, these geological domains are represented by the Mesozoic Río Damas, Baños del Flaco and Colimapu Formations and the Cenozoic Abanico Formation. This major tectonic boundary has been interpreted as the eastern border of Abanico extensional basin (Piquer et al. 2010; Charrier et al. 2002), developed during the Eocene to the Early Miocene (Giambiagi et al. 2015). According to Piquer et al. 2015, the Abanico basin was compartmentalized by previous regional-scale normal fault systems striking NW and NE. Later, during the inversion of Abanico basin, those faults were selectively reactivated by the Mio-Pliocene east–west contraction, with the NW-striking faults showing a composite reverse-sinistral movement and the NE-striking faults showing mainly dextral strike-slip movement. As a consequence of this compressional tectonic event, a fault and thrust belt was developed toward the back-arc accommodating

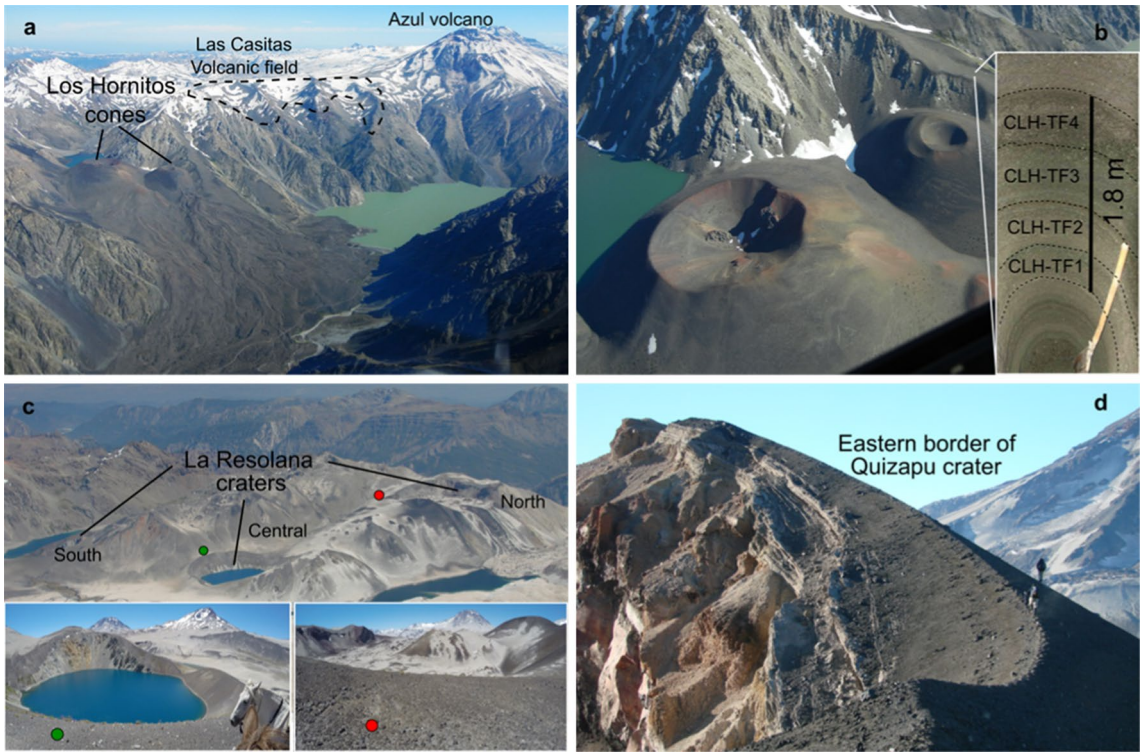

Fig. 5 **a** Panoramic view looking northward. In the foreground the two cones of Los Hornitos and its lava field. In the background segmented line is showing the location of Las Casitas volcanic field and Azul volcano. **b** Aerial view of the two cones of Los Hornitos showing the preservation state. Also is shown the inset with the excavated section of the tephra deposit from the initial explosive stage of the younger (eastern) cone. **c** Panoramic view looking west showing the distribution of La Resolana craters. The north crater is composed by pyroclastic and lava effusion, while only pyroclastic deposits are found associated with the central and south craters. *Green* and *red points* show the positions of observer for the *lower inset*. **d** Northward view of the eastern rim of Quizapu crater showing the tephra deposit of mafic scoria emitted in the terminal stage of the plinian event of 1932

different amounts of crustal shortening along the orogen (e.g., Giambiagi et al. 2015; Mescua et al. 2014).

At local scale, LHC are situated in the southern tip of a NNW valley, which represents the contact between the strongly folded volcano-sedimentary rocks of Abanico Formation to the west and the 12–7 Ma La Invernada pluton (Astaburuaga 2014; Hildreth and Drake 1992) to the east (Figs. 3a, b, 4). Therefore, field observations and tectonic interpretations suggest that monogenetic vents occurring at the western border of DGVF (Fig. 1c) are located over a tectonically weak zone that during Miocene to Early Pliocene time, under a compressive regime, allowed the emplacement of La Invernada pluton and absorbed certain amounts of compressive deformation (e.g., Astaburuaga 2014), probably facilitated by the thermal gradient provided by the intrusives. Compressive stresses gradually decreased from the Early Pliocene to today (Giambiagi et al. 2015). As a consequence, a thick, mostly mafic volcanic sequence, the Cola de Zorro Formation, was emplaced along the arc region between 36° and 39°S during Late Pliocene to Pleistocene (Sellés 2006; Muñoz and Niemeyer 1984; Vergara and Muñoz 1982).

Sampling and analytical methodology

Samples for whole-rock and mineral chemistry analysis were taken from different eruptive units (tephra, bomb and lava) at LRC and LHC and from the terminal mafic scoria of 1932 eruption of Quizapu volcano (TQZV). At Los Hornitos cones, stratigraphic relations and preservation state indicate the East cone to be the younger cone. A widely distributed tephra deposit covers the area reaching up to ~1.5 km around the cones. This fallout deposit represents the initial (explosive) eruptive stage of LHC-East and is comprised of layered beds of variable thickness and amounts of lapilli and ash fragments. At the excavation site (~400 m E from the vent), individual layers have a maximum thickness of ~50 cm. Samples were collected at four different depths within the section, as shown in the inset of Fig. 5b. Olivine is the most common mineral phase in the tephra layers and occurs as loose grains, simplifying their separation. The terminal scoria of the 1932 Quizapu eruption ranges from 2 to 6 m (Fig. 5d) in thickness. It overlies finely laminated phreatic ash deposits (Hildreth and Drake 1992). The contact between phreatic and mafic scoria tephra is gradational suggesting

a continuous eruption of these deposits and a progressively larger contribution from mafic magmas. The terminal scoria is generally coarsening upward to lapilli size with the uppermost 2 m mostly composed of glassy, highly vesiculated mafic scoria lacking earlier erupted phreatic components. Some larger mafic bombs (>20 cm) are found on the crater rim. These deposits are restricted to the east side of the crater. We collected samples from the upper part of the deposit.

Olivine separation was performed at the Laboratory of Sedimentology, Universidad de Concepción, Chile, using a combination of magnetic (Frantz isodynamic magnetic separator) and gravity (2.96 and 3.10 g/cm^3 dense liquids) techniques and mounted in epoxy for chemical analysis, while olivine crystals from the lavas were analyzed in thin sections. At LHC, olivine was concentrated from the ash-rich sample (CLHE-TF2; Fig. 5b). Additionally, a coarse lapilli-rich sample (CLHE-TF4; Fig. 5b) was selected for whole-rock analysis. Thin sections were prepared for olivine analysis from the late effusive stage at LHC (lava sample CLHE-2) and from massive rock samples (i.e., slabby blocks, lava and bombs) from LRC-North and South.

Bulk rock major and trace element analyses were performed by X-ray fluorescence (XRF) at Washington State University following the procedure of Johnson et al. (1999), and results were previously published by Ruprecht et al. (2012). Olivine mineral chemistry was obtained using a JEOL 733 electron microprobe and a JEOL JXA8600 electron microprobe at the University of Washington (Seattle) and at the Instituto de Geología Económica Aplicada (GEA) from the Universidad de Concepción (Chile), respectively, with similar beam conditions (15 kV accelerating voltage, 20–30 nA beam current and a 5 μm beam diameter). Reference materials for calibration on the JEOL 733 were fayalite (Si, Fe), garnet (Mn), clinopyroxene (Ca), forsterite (Mg) and NiO (Ni) with counting times of 40/20 s (peak/background) for all elements except 100/50 s for Ca. On the JEOL JXA8600, spectrometers were calibrated on diopside USNM 117733 (Si) and fayalite USNM 85276 (Fe) (Jarosewich et al. 1980) and synthetic MnTiO3 (Mn), forsterite (Mg), wollastonite (Ca) and NiO (Ni). Counting times were 20/10 peak/background for Si, Mg and Fe and 120/60 for Ca, Mn and Ni. Analytical precision was typically better than 1 % for Si, Mg and Fe, better than 5 % for Mn and Ca and better than 7 % for Ni (20 % for JEOL 733). Data reduction was performed using the ZAF correction method.

Results

Vent distribution and structural controls

At regional scale, the segment between 35.5° and 36.5°S, where mafic volcanism is present, comprises an area of about 5000 km^2, bounded by the DGVF to the north and by the Nevado de Longaví and Chillán volcanoes to the south (Fig. 1b). The overall distribution of mafic volcanic units in this segment can be organized from north to south as follows:

1. A cluster of at least 11 vents and volcanic products outcropping in the west flank of DGVF. This includes Manantial Pelado (MPC, 5 vents), LRC (3 maar-like vents), LHC (2 cones) and Las Casitas volcanic field (CAS) (Fig. 1c).
2. A cluster of at least 30 vents or volcanic units distributed in the north and west flank of LdM (Fig. 2). This includes several units accounting since the Early Pleistocene and has been described by Hildreth et al. (2010). Here, several silicic andesite units have been excluded from the analysis, and only basaltic and basaltic andesite compositions are considered.
3. Three isolated and poorly known volcanic centers are dispersed at the southern edge of the segment (Fig. 2). The Loma Blanca (LBL) and Rezago (RZG) volcanoes are two monogenetic centers located in the southeast area of Nevado de Longaví volcano (NLV). Their state of preservation suggests a Late Pleistocene and post-glacial age, respectively. Additionally, the Villalobos volcano corresponds to a mafic stratocone of Early Pleistocene age located 10 km south of NLV (Sellés 2006).

Locally the five monogenetic vents in the northern cluster (1) occurring at the southwestern side of DGVF align along a NNW–SSE lineaments (Figs. 1c, 4). Therefore, vents of LRC-North and Central coincide with CAS southward, while the LRC-South aligns with LHC vents southward by the NNW–SSE valley of Los Hornitos. The distribution of these vents seems to be also controlled by NE–SW lineaments, since most cones occur at these lineament intersections. These two structural trends dominate in the SVZ segment between 35° and 37°S (Figs. 1b, c, 2).

The southward prolongations of NNW–SSE lineaments reach the central portion of LdM, and at its northwestern periphery, they intersect the locally dominant NE–SW to ENE–WSW lineaments (Fig. 2). Toward the southwestern margin of LdM, the Hoyo Colorado cone (BHC) together with the older Cajón Rodríguez vents (MCR) are emplaced above a lineament that intersects the northern flank of Pellado volcano through the north (Fig. 2). Several older mafic volcanic units at the western periphery of LdM seem to be grouped in this setting of structures, where a corridor of ENE–WSW lineaments occurs and probably controls the emplacement of these mafic volcanoes (Fig. 2).

Toward the southern edge of the segment, another NNW–SSE lineament that flanks the eastern border of Nevado de Longaví volcano (NLV) additionally contains the Loma Blanca and Rezago volcanoes through the south. Further,

Villalobos volcano (Sellés 2004; VLO) is emplaced near the intersection of NNW–SSE and NE–SW lineaments (Fig. 2).

The NNW–SSE lineaments seem to be the main control in the distribution of mafic volcanism between 35.5° and 36.5°S.

Relative age of mafic volcanoes

Table 1 summarizes the age of 38 mafic monogenetic vents recognized in the segment between 35.5° and 36.5°S. The relative distribution is divided into four groups based on published ages and preservation state of volcanic landforms:

Group 1 The oldest dated units belong to the Early Pleistocene and correspond to Botacura (MVB; 1324 ka) and Aguirre (MVA; 1290 ka) volcanoes (Hildreth et al. 2010) (Fig. 2). The undated volcanism of Cordón Filume (MCF; Fig. 2), however, could be even older than 1.5 Ma, as suggested by Hildreth et al. (2010). According to those authors, at least eight mafic volcanic units belong to this period. Further, the mafic Villalobos volcano in the vicinity of NLV has been dated in the range of about 1.7–0.9 Ma (Sellés 2006).

Group 2 At least 13 volcanic units are defined for the Middle Pleistocene, that among others centers include the Cerro San Pedro volcanic shield (MCS; 243 ka), Pellado (PEV; ~188–83 ka) and Cerro Campanario (MCC; ~150 ka) volcanoes (Hildreth et al. 2010). At a broadly similar period, the volcanism was active at Las Casitas (CAS) volcanic field, whose age range between 0.51 and 0.34 Ma (Wolff 2005, 2008). Further, at the Tatara–San Pedro complex, the Middle El Molino Sequence (MEM; 579 ka) includes three primitive basaltic compositions and an evolved basaltic lava (Dungan et al. 2001).

Group 3 During the Late Pleistocene, at least ten mafic units developed in the LdM. Those are represented by Estero Bobadilla mafic andesite (MEB; 86 ka), El Candado basalt (BEC; 62 ka) and Vega Piedras Negras andesite (MPN; 54 ka) (Hildreth et al. 2010). Additionally, the undated units of Manantial Pelado cluster (MPC; Fig. 1c), at the DGVF, and Loma Blanca vent (LBL), at the southern extreme of the segment, are suggested to have erupted during this period.

Group 4 Finally, the distribution of post-glaciation vents (<25 ka) occurs along the whole segment. From north to south, these well-preserved cones include: LRC and LHC at DGVF; the Arroyo Cabeceras de Troncoso (MCT), Crater 2657 (MCP) mafic andesites and the scoria cone of Hoyo Colorado basalt (BHC), all present at the LdM. Lastly, the isolated Rezago volcano (RZG) belongs to this group and is located at the southern limit of this segment.

Table 1 Summary of mafic volcanic units and vents located between 35.5° and 36.5°S

Group	Volcanic unit		Relative age		
Group 4	Los Hornitos	LHC	0.025 Ma	Holocene	
	La Resolana	LRC			
	Cabecera Troncoso	MCT*			
	Crater 2657	MCP*			
	Hoyo Colorado	BHC*			
	Rezago	RZG			
Group 3	Loma Blanca	LBL	0.126 Ma	Late	Pleistocene
	Manantial Pelado	MNPC			
	El Candado	BEC*			
	Vega Piedras Negras	MPN*			
	Cajón Rodríguez south	MCR*			
	Laguna Turbia	MLT*			
	Salto del Maule	MSM*			
	Estero Bobadilla	MEB*			
	Puente de la Laguna	MPL*			
	Las Salinas	MLS*			
Group 2	Las Casitas	CAS	0.9 Ma	Middle	
	Volcán de la Calle	MVC*			
	Cerro Campanario	MCC*			
	Volcán Pellado	PEV			
	Cerro San Pedro	MCS*			
	Cerro Bahamondes	MCB*			
	La Poza	MLP*			
	Bobadilla Chico	BBC*			
	Paso Campanario	MPC*			
	Río Blanco	MRB*			
	Oeste Cerro Risco Bayo	MOR*			
	Cajón Filume	BCF*			
	Mid El Molino Sequence	MEM			
Group 1	Cordón Filume	MCF*	2.6 Ma	Early	
	Volcán Aguirre	MVA*			
	Volcán Botacura	MVB*			
	Sin Puerto	MSP*			
	Volcán Ñirales	MVÑ*			
	Volcán Munizaga	MVM*			
	Arroyo Santuario	MAS*			
	Quebrada Fiera	MQF*			
	Villalobos	VLO			

Only basaltic and basaltic andesite (SiO_2 < 57 wt%) compositions have been considered. Several silicic andesite compositions from LdM have been excluded of this analysis. Preservation state of volcanic units of Group 4 indicates a post-glacial age, which had been determined to begin at ~25 ka in the area of Laguna del Maule at ~36°S in central Chile (Singer et al. 2000)

Petrography

La Resolana craters (LRC)

Eruptive products from these vents, including slabby blocks, bombs and lava samples are characterized by a low proportion of phenocrysts (~15–20 vol%), which consist of olivine (5–8 vol%) and minor amounts of plagioclase (~4–5 vol%) and clinopyroxene (3–7 vol%). The groundmass (~80–85 vol%) is dominated by plagioclase microlites (~55 vol%) with minor proportions of clinopyroxene (~7 vol%), olivine (~6 vol%), magnetite (~7 vol%) and glass (~10–30 vol%) (Table 2). The lavas from LRC-North contain orthopyroxene as a fine rim surrounding olivine phenocrysts and also as independent micro-phenocrysts in the groundmass. Those rims may result from the

Table 2 Summary of mineral phases occurring in the sampled volcanic units

	LHC			LRC			TQZV
	Lava W cone	Lava E cone	Tephra E cone	Bomb N cone	Lava N cone	Bomb S cone	Tephra 1932
Phenocrysts (%)	16	15	30	15	20	15	22
Ol	10	12	30	8	8	5	7
Plg	5	3		4	5	3	10
Cpx	3	5		3	3	7	
Opx					4		2
OxiHbl							3
Groundmass (%)	84	85	70	85	80	85	78
Glass	7	5	7	10	10	30	48
Microlites	77	80	63	75	75	55	30

Mineral phases occurring in different volcanic units of studied vents. Mineral nomenclature is as follows: *Ol* olivine, *Plg* plagioclase, *Cpx* clinopyroxene, *Opx* orthopyroxene, *OxiHbl* oxyhornblende

reaction between olivine and melt during a normal basalt-to-andesite crystallization sequence (e.g., Sisson and Grove 1993; Grove et al. 1997).

Los Hornitos cones (LHC)

The analyzed lapilli-poor tephra bed (sample CLHE-TF2; Fig. 5b) is olivine rich and represents the only phenocryst phase observed in the separates. Olivine phenocrysts are medium to coarse grained (250–700 μm), euhedral to subhedral in shape and frequently contain Cr-spinel inclusions. Hand-magnet separation revealed a great proportion of fine-grained (<200 μm) magnetite; however, the loose grains are also a mix with other phases. A glassy groundmass with plagioclase microlites and minor olivine crystals usually surround these olivines. In addition, a minor population of small (<150 μm) crystals of clinopyroxene is often observed as loose grains in the separates.

The mineralogical analysis of the sample CLHE-TF4 indicates the presence of forsterite-rich olivine and Cr-spinel inclusions as the dominant phases. Detailed mineral chemistry of olivine is presented below.

The late effusive stage of this vent emitted a voluminous lava flow with variable phenocryst proportions (15 and 20 vol%) including olivine (~12 vol%) and a lesser amount of clinopyroxene (~5 vol%) often clustered in crystal agglomerates. A minor proportion of plagioclase is observed as elongated micro-phenocrysts (~3 vol%). The groundmass is almost holocrystalline (80–85 vol%) with plagioclase (~48 vol%), clinopyroxene (~28 vol%), magnetite (~5 vol%) and a minor amount of glass (~4 vol%).

Terminal mafic scoria from Quizapu volcano (TQZV)

The mafic fallout deposit of Quizapu volcano is mostly composed by ash (75 vol%) and lapilli fragments (25 vol%), with a scarce occurrence of bombs (Fig. 5d). The phase assemblage in the analyzed tephra sample is mainly composed of magnetite (30 vol%, representing a mix with other phases) and glass (48 vol%), with minor amounts of plagioclase (10 vol%), olivine (7 vol%), orthopyroxene (2 vol%), oxyhornblende (3 vol%) and apatite (<1 vol%) (Table 2). Crystals often exhibit a fragmental texture with crystal fragment sizes less than 220 μm.

Whole-rock chemistry

Based on geochemical results presented by Ruprecht et al. 2012 (performed on the same samples studied here) and Hildreth and Drake (1992) (Table 1, electronic supplementary data), the analyzed samples ($n = 16$) are mostly basaltic andesite in composition with SiO_2 contents ranging between 53.5 and 55.0 wt%. The only exceptions are the CLHE-TF4 sample, which is of basaltic composition ($n = 1$, see below for details), and sample Q-9, corresponding to an andesite composition. Erupted magmas have a sub-alkaline character based on the canonical TAS diagram (Fig. 6). Besides, the geochemical data yield a modified alkali-lime index (MALI) ranging between −5.32 and −2.64, a mean FeO*/MgO ratio of 1.36 ($n = 15$; Fig. 7) and a K_2O content lower than ~2.07 wt%, typical of medium-K, calc-alkaline suites.

The coarse lapilli-rich tephra (sample CLHE-TF4, Fig. 5b) from the initial explosive stage at LHC yields highly anomalous values of MgO (13.7 wt%), Cr (1209 ppm) and Ni (347 ppm), but a relatively evolved character when considering the SiO_2 (51.5 wt%) content (Fig. 7).

Despite the common basaltic andesite composition among the eruptive products, rocks from LHC and LRC are less evolved compared with the terminal scoria at Quizapu volcano (TQZV), where MgO contents are lower for a similar SiO_2 content.

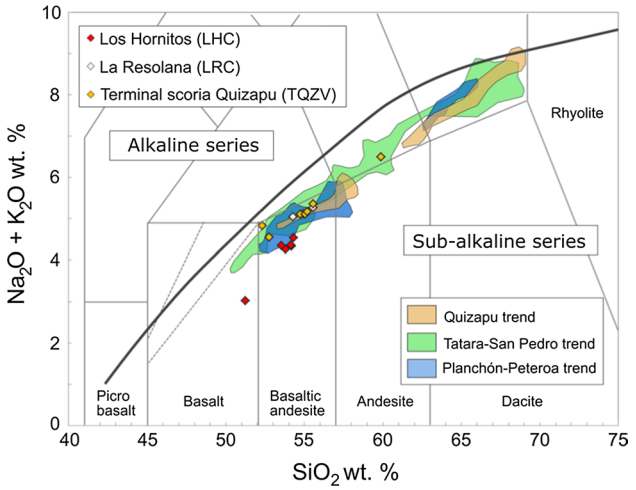

Fig. 6 TAS diagram showing the whole-rock contents of studied samples compared to chemical trends of neighbor volcanic centers. LHC samples display systematic depletion in alkalis compared to LRC and TQZV samples. Data for neighbor volcanic centers were obtained from EarthChem (October 2015) and complemented with data provided by Ruprecht et al. (2012) and Tormey et al. (1995). Fields were plot using the 95 % of samples for Planchón–Peteroa and Tatara–San Pedro volcanic complexes

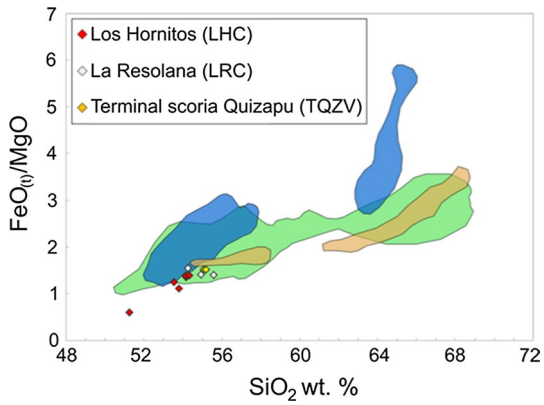

Fig. 7 FeO(total)/MgO ratio in whole-rock elemental contents in analyzed samples. LHC display a slightly lower ratio compared with TQZV and LRC. *Color fields* represent the same as in Fig. 6

Olivine composition

Considering crystal-chemical and textural criteria, magmatic phenocrysts (sensu stricto) correspond to large crystals that grew from the melt in which they were erupted. Nevertheless, in a textural-alone terminology, phenocrysts (sensu lato) and microlites refer to crystal sizes, regardless of the origin of crystals. Here, we use the latter meaning, since determining a genetic relation between crystals and co-erupted melts (sensu stricto) is often difficult to confirm.

At LHC the olivine populations from the initial (explosive) and late (effusive) stage are compositionally different although both are normally zoned. Olivine phenocrysts from the initial explosive stage are more forsteritic (>~ Fo_{85}) than those from the effusive stage (<~Fo_{85}) (Fig. 8a, b; Table 2, electronic supplementary data). The olivine cores of these two olivine groups exhibit an increasing forsterite range from 2.2 Fo units in the initial tephra (Fo_{90} to $Fo_{92.2}$) to 8 Fo units in the lava flows (Fo_{77} to Fo_{85}). The Fo and Ni contents decrease from the initial tephra ($Fo_{90–92.2}$ and ~1800–3642 ppm Ni, respectively) to the late lava flows ($Fo_{77–85}$ and ~380–1095 ppm Ni).

A large fraction of olivine measurements comprise a narrow range from Fo_{87} to Fo_{92} ($n = 50$) in the initial stage (tephra) with only a few measurements with lower Fo content (Fo_{79} to Fo_{87}; $n = 6$). Those lower values correspond to a thin overgrowth present in some olivine phenocrysts. The Ni and Fo contents correlate positively and display a steep variation pattern, with Ni varying from 3642 to 651 ppm for a narrow range of forsterite from ~Fo_{92} to Fo_{88} consistent with olivine-dominated fractional crystallization (Fig. 8a). Olivine from the initial stage at LHC often contains Cr-spinel inclusions, with Cr# [defined as the atomic ratio of Cr/(Cr + Al)] ranging from 76 to 60 (unpublished data).

On the other hand, the full compositional range of olivine phenocrysts from the late stage (lava flow) varies from Fo_{64} to Fo_{85} with Ni contents lower than 1095 ppm ($n = 32$) (Fig. 8a).

Fo contents of olivine from LRC are intermediate when compared with those from the effusive stage at LHC and Quizapu volcano (mafic scoria), and range from Fo_{68} to Fo_{83}, with Ni contents lower than 1212 ppm ($n = 51$) (Fig. 8a). Conversely to the case of monogenetic vents, olivine phenocrysts from the terminal mafic scoria of Quizapu volcano (TQZV) exhibit a reversely zoned core-to-rim pattern, with forsterite values in the range of Fo_{81} to Fo_{65}, with Ni contents lower than 1071 ppm ($n = 131$) (Fig. 8a).

The content of Ca in all analyzed olivine crystals varies from about 700–1900 ppm, and it shows a systematic increase with decreasing forsterite content (Fig. 8b). The Ca–Fo diagram shows at least two different variation trends, where the high-Fo olivine population displays a steeper Ca enrichment (Fig. 8b).

Discussion

Olivine composition as indicator of parental melt

Olivine composition can be used as probe of parental melt composition because at most crustal pressures olivine is the first phase to crystallize in almost all mantle-derived magmas (e.g., Weaver et al. 2011). This mineral is also useful because its compositional variation (e.g., Mg/Fe, Ni, Cr, Ca) is suitable for monitoring the degree of

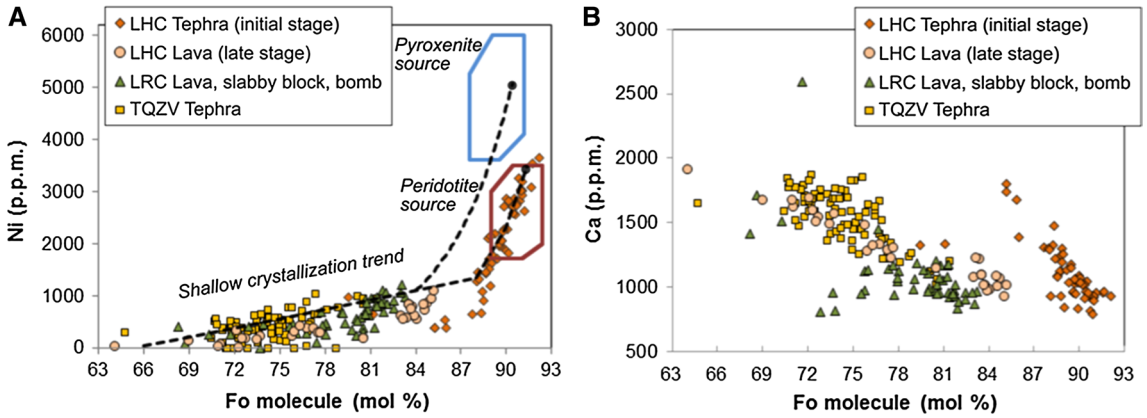

Fig. 8 **a** Forsterite molecule (Fo) versus Ni (ppm) in olivine from the studied eruptive centers. Olivine from the initial tephra at LHC displays a narrow range in Fo for a wide variation in Ni contents (from 3642 to ~600 ppm) constituting the olivine-dominated crystallization trend. A great proportion of these data plots in the calculated olivine composition to be in equilibrium with a peridotite source. Pyroxenite source is also plotted for comparison (Straub et al. 2011). Fractionation curves for two different primary melt compositions are provided (Ruprecht and Plank 2013). Olivine composition from LHC lavas, LRC and TQZV constitutes the shallow crystallization trend given by a wide range in Fo (Fo < 87) and Ni contents lower than ~1200 ppm. **b** Forsterite molecule (Fo) versus Ca (ppm) in olivine showing separated evolution trends for high-Fo olivine (Fo > 85) from the initial stage at LHC and the shallow trend crystallization depicted by LHC lavas, LRC and TQZV

fractional crystallization (or differentiation) of the parental magma.

Olivine from the initial explosive stage at LHC displays the highest Fo and Ni contents of all analyzed samples. A few (~6 vol%) of these olivines can be classified as ultramagnesian (Fo > 91.5; e.g., Keiding et al. 2011). Primitive magnesian olivine (Fo > 88) is considered to be in equilibrium with the mantle and thus expected to be associated with primitive mantle-derived melts. As shown in Fig. 8a, the bulk composition of most olivine phenocrysts from the initial stage of LHC is in the range of olivines from a peridotitic mantle source (e.g., Straub et al. 2011). The fact that most of the LHC olivines are $>Fo_{88}$ with Ni contents up to more than 3600 ppm suggests that they are the Mg-rich liquidus phase. Compositional variations in Ca and Ni in such magnesian olivine (Fo > 88; Fig. 8a, b) are also consistent with olivine-dominated fractional crystallization. The evolution trend defined by lower values (Fo < 88, Ni < 1212 ppm) is consistent with a lower pressure and temperature crystallization where plagioclase and clinopyroxene, seen as microlites in the groundmass, co-crystallize with olivine. Crystallization of plagioclase at high crustal levels increases the CaO/Al_2O_3 ratio and alkalis ($Na_2O + K_2O$) content in the melt favoring the Ca incorporation in olivine, as suggested by Libourel (1999).

Following this reasoning, composition of olivine crystals from LRC and Quizapu volcano would indicate a low-pressure shallow crustal evolution from a more differentiated melt compared with that associated with LHC. Olivine phenocrysts from the lava flow at LHC, however, share a similar evolution trend with the LRC and Quizapu volcano olivines (Fig. 8a, b). In this context, three major possibilities arise for LRC and Quizapu volcano melt history: (a) Both volcanic vents could have erupted more forsteritic and Ni-rich olivine during the initial explosive stage, but these were buried by later volcanic products, as the case of LHC. This alternative is particularly relevant for LRC due to a more similar setting to LHC. (b) The magmatic plumbing system of LRC and Quizapu volcano is more complex than LHC and forsteritic olivine did not reach the surface. (c) The magmatic systems of LRC and Quizapu volcano were fed by more evolved melts.

The highly anomalous contents of MgO, Ni and Cr in the coarse lapilli-rich sample (CLHE-TF4) from the initial stage at LHC are interpreted as result of a high proportion of forsterite-rich olivine in the sample. Similar chemical anomalies have been found in lava and dike samples (unaffected by eolian fractionation), but containing high proportions of antecrysts, which are large crystals that according to their chemical composition may not have shared common histories or crystallized from the magma in which they are now hosted, but rather may have grown within the same magmatic system but in a more primitive magma than that from which they are found (Larrea et al. 2013). Thus, although the whole-rock composition of the ash-rich level (sample CLHE-TF2; Fig. 5b) hosting the Mg-rich olivines is not known, the closely related coarse lapilli deposit has a basaltic composition (~13.7 wt% MgO and 51 wt% SiO_2; Table 1, electronic supplementary data). Therefore, the primitive character of this tephra deposit from LHC may be a primary feature of a poorly evolved phyric melt containing about 20 vol% of high-forsterite olivine, which has

experienced limited crystallization at shallow crustal depths involving plagioclase and clinopyroxene. Similar primitive whole-rock compositions have been reported for other monogenetic volcanoes such as Jorullo in Mexico (Johnson et al. 2008). Although other volcanic rocks at LHC, mostly lava flows, are basaltic andesites, at the nearby LdM Mg-rich basaltic rocks have also been reported for a couple units (Hildreth et al. 2010).

Furthermore, for primitive olivine like those from LHC, thermal considerations regarding the high-Mg (Fo > 88) compositions and Ni diffusion in olivine would require a very short crustal residence time—months to few years at most—in order to prevent a re-equilibration toward more evolved compositions (Ruprecht and Plank 2013). This contrasts with those olivines from the other mafic rocks of the DGVF, where Ni and Fo contents are lower than ~1200 ppm and ~85 in olivine crystals, respectively.

Structural control of mafic volcanism between 35.5° and 36.5°S

The NNW–SSE set of lineaments is a regional feature observed between ~35° and ~37°S that have also been noted by other authors to dominate over the NS and NE alignments of volcanic centers in the transitional SVZ (e.g., López-Escobar et al. 1995). The pattern defined by NNW–SSE lineaments is broadly in agreement with pre-Andean oblique-slip structures (e.g., high angle faults in the basement) proposed by Cembrano and Lara (2009) to control the position of some volcanic edifices and associated flank vents, as the case of Chillan volcanic chain (~36.8°S).

On the other hand, north of 37°S, the active volcanic front is emplaced above margin parallel, reverse faults developed either within Mesozoic units or at the boundary between Cenozoic and Mesozoic volcano-sedimentary sequences in the westernmost portion of the fold and thrust belt of the back-arc. This is the case of Maipo and Planchón–Peteroa volcanic complexes, respectively. Southward, Descabezado Grande-Azul-Quizapu volcanic complex is located at the Meso-Cenozoic boundary above Cenozoic intrusive basement (e.g., Astaburuaga 2014).

The segment between 35.5° and 36.5°S is located in a transitional zone where the Meso-Cenozoic cover diminishes toward the south. This cover attenuation may reduce, or even prevent in some cases, the possibility that magmas on route to the surface became trapped at the basement–cover discontinuity, where protracted differentiation processes can take place.

According to Cembrano and Lara (2009), both structural controls (margin parallel and NW–SE structures) are kinematically uncoupled to the present-day tectonic environment and rather the spatial distribution and overall morphology of individual volcanoes and groups of volcanoes are primarily controlled by the inherited basement structures that underlie this arc segment. Therefore, the combination of a reduced Meso-Cenozoic volcano-sedimentary cover and deep inherited structures reaching high crustal levels, may have contributed for the widespread mafic effusive centers emplacement in the SVZ between 35.5° and 36.5°S.

Further, monogenetic volcanism is favored in extensional settings. In convergent margins, the structural control may vary significantly, involving compressive, strike-slip, extensional and oblique systems (Nakamura 1977; Acocella 2014). In the SVZ, the significant degree of strike-slip deformation along the arc, even in the northern (NSVZ) and transitional (TSVZ) segments, allows that compression and extension can occur at same time but in different orientations, both oblique to the magmatic arc trend (Cembrano and Lara 2009). In this setting, an additional factor enhancing the dike propagation and eruption is the occurrence of extensional co-seismic and post-seismic deformation triggered by a megathrust earthquake in the forearc (Lupi and Miller 2014; Bonali et al. 2015). This transient variation of the stress field in the overriding plate may shift from compressive to extensional, as evidenced by the occurrence of normal faulting along a NNW–SSE trend, triggered by the Mw = 8.8 Maule earthquake in 2010 in South-Central Chile (Farías et al. 2011) and the geodetically detected during and immediately after the 2011 Tohoku earthquake, Japan (Ozawa et al. 2011; Takada and Fukushima 2013). In particular, dike intrusion during these transient conditions may occur along otherwise non-favorable orientations, as arc oblique-NNW–SSE, perpendicular to the oblique convergence vector at the SVZ (Acocella 2014).

On the other hand, Piquer et al. 2015 propose that the intersection of two conjugates set of regional faults, the NE-striking dextral and the NW-sinistral striking faults can generate a dilatational environment along NW-trending structures during the incremental motion of the NE-striking faults under east–west compression, thus explaining the NNW–SSE trend of breccias and ore bodies at Rio Blanco–Los Bronces and El Teniente porphyry deposits (see Piquer et al. 2015 for details).

Finally, as a remarkable fact, the NNW–SSE and ENE–WSW trends are broadly concordant with the ancient structures that controlled the Late Triassic–Early Jurassic rift systems (Ramos 2009) that were reactivated during the rifting event associated with the opening of the South Atlantic Ocean in the early Cretaceous (Jacques 2003; Ramos 2009). Furthermore, those structural trends have been observed as major features in the entire South American continent, acting as weakness zones which can be repeatedly reactivated, playing a major role in the tectonostratigraphic evolution of the continent (Jacques 2003). The deep and penetrative character of such structures would

explain their effectiveness in channeling and transporting deep-seated mafic magmas through the crust.

We speculate that a decrease in the compressional stress regime in the arc region, related to a transient post-seismic relaxation after large subduction earthquakes (e.g., Lupi and Miller 2014; Bonali et al. 2015), is a possible explanation to link the structural pattern observed in the distribution of mafic volcanoes between 35.5° and 36.5°S.

Conclusions

The primitive character of olivine phenocrysts from the initial stage at LHC is interpreted to result from the crystallization of a primitive melt in deep crustal or mantle environments, where olivine (±spinel) constitutes the only crystallizing phases. Compositional variations in the more forsteritic (Fo > 88) and Ni-rich olivine phenocrysts (Ni > 650 ppm) suggest equilibrium with a peridotite source. The later joining of shallow crystallization phases, as plagioclase and clinopyroxene, co-crystallizing together with olivine in the groundmass, modifies the olivine-dominated compositional trend (Fig. 8a, b). Composition of olivine crystals from LRC and Quizapu volcano would indicate a low-pressure shallow crustal evolution from a more differentiated melt compared with that associated with LHC.

Limited residence times in crustal levels are needed in order to preserve the compositional zonation of such forsterite-rich olivine to prevent elemental diffusion at magmatic temperatures. The structural setting where Los Hornitos mafic cones are located suggests that the NNW-striking structures may represent the deep crustal structures that facilitated the rapid ascent of these mafic magmas through crust. These structures, inherited from ancient tectonic regimes, may have also played an important role in the transport of mafic magmas through the Andean crust in the revised segment (35.5°–36.5°S) during post-Pliocene times, allowing the northernmost presence in the SVZ of near primitive magmas at the surface.

Thus, the widespread emplacement of Pleistocene to Holocene monogenetic mafic vents in the TSVZ, between 35.5° and 36.5°S, is controlled by the occurrence of NNW–SSE and NE–SW deep pre-Andean structures. The combination of a reduced Meso-Cenozoic volcano-sedimentary cover and such structures may have provided a more direct pathway for primitive magma ascent.

Acknowledgments We would like to thank especially G. Bergantz for enabling a 3-month research visit to the University of Washington for P. Salas, during which significant parts of the data were produced. Hugo Neira and Daniela Astaburuaga are sincerely acknowledged for their valuable contribution in GIS support and structural discussions, respectively. P. Salas was supported during part of the project by Beca Postgrado 2015 from Universidad de Concepción. P. Ruprecht gratefully acknowledges funding from the U.S. National Science Foundation (Grants EAR-1347880 and EAR-1426820). We would like to thank Dr. Verónica Pineda for providing facilities for mineral separation at the Laboratory of Sedimentology, Universidad de Concepción, Chile. Charles Stern and Francisco Gutierrez provided helpful reviews of this manuscript.

References

Acocella V (2014) Structural control on magmatism along divergent and convergent plate boundaries: overview, model, problems. Earth Sci Rev 136:226–288

Annen C, Blundy JD, Sparks RSJ (2006) The genesis of intermediate and silicic magmas in deep crustal hot zones. J Petrol 47(3):505–539

Astaburuaga D (2014) Evolución estructural del límite Mesozoico-Cenozoico de la Cordillera Principal entre los 35°30′ y 36° S, Región del Maule, Chile. Master thesis. Universidad de Chile

Bonali FL, Tibaldi A, Corazzato C (2015) Sensitivity analysis of earthquake-induced static stress changes on volcanoes: the 2010 Mw 8.8 Chile earthquake. Geophys J Int 201(3):1868–1890

Bucchi F, Lara LE, Gutiérrez F (2015) The Carrán–Los Venados volcanic field and its relationship with coeval and nearby polygenetic volcanism in an intra-arc setting. J Volcanol Geoth Res 308:70–81

Cembrano J, Lara L (2009) The link between volcanism and tectonics in the southern volcanic zone of the Chilean Andes: a review. Tectonophysics 471(1):96–113

Charrier R, Baeza O, Elgueta S, Flynn J, Gans P, Kay S, Zurita E (2002) Evidence for Cenozoic extensional basin development and tectonic inversion south of the flat-slab segment, southern Central Andes, Chile (33–36 SL). J South Am Earth Sci 15(1):117–139

Dungan MA, Wulff A, Thompson R (2001) Eruptive stratigraphy of the Tatara-San Pedro complex, 36°S, Southern Volcanic Zone, Chilean Andes: reconstruction method and implications for magma evolution at long-lived arc volcanic centers. J Petrol 42(3):555–626

Farías M, Comte D, Roecker S, Carrizo D, Pardo M (2011) Crustal extensional faulting triggered by the 2010 Chilean earthquake: the Pichilemu seismic sequence. Tectonics 30(6):1–11

Genareau K, Valentine GA, Moore G, Hervig RL (2010) Mechanisms for transition in eruptive style at a monogenetic scoria cone revealed by microtextural analyses (Lathrop Wells volcano, Nevada, USA). Bull Volc 72(5):593–607

Giambiagi L, Tassara A, Mescua J, Tunik M, Alvarez PP, Godoy E, Tapia F (2015) Evolution of shallow and deep structures along the Maipo–Tunuyán transect (33°40′S): from the Pacific coast to the Andean foreland. Geol Soc Lond Spec Publ 399(1):63–82

Grove TL, Donnelly-Nolan JM, Housh T (1997) Magmatic processes that generated the rhyolite of Glass Mountain, Medicine Lake volcano, N. California. Contrib Mineral Petrol 127(3):205–223

Higgins MD, Voos S, Vander Auwera J (2015) Magmatic processes under Quizapu volcano, Chile, identified from geochemical and textural studies. Contrib Miner Petrol 170(5–6):1–16

Hildreth W, Drake RE (1992) Volcán Quizapu, Chilean Andes. Bull Volcanol 54(2):93–125

Hildreth W, Moorbath S (1988) Crustal contributions to arc magmatism in the Andes of central Chile. Contrib Miner Petrol 98(4):455–489

Hildreth W, Godoy E, Fierstein J, Singer B (2010) Laguna del Maule Volcanic field: eruptive history of a Quaternary basalt-to-rhyolite distributed volcanic field on the Andean range crest in central Chile. Servicio Nacional de Geología y Minería-Chile, Boletin 63:142

Jacques J (2003) A tectonostratigraphic synthesis of the Sub-Andean basins: implications for the geotectonic segmentation of the Andean Belt. J Geol Soc 160(5):687–701

Jarosewich E, Nelen JA, Norberg JA (1980) Reference samples for electron microprobe analysis. Geostand Newsl 4(1):43–47

Johnson DM, Hooper PR, Conrey RM (1999) XRF analysis of rocks and minerals for major and trace elements on a single low dilution Li-tetraborate fused bead. Adv X-ray Anal 41(843867):1988

Johnson E, Wallace P, Delgado Granados H, Kent A (2008) Magmatic volatile contents and degassing-induced crystallization at Volcán Jorullo, Mexico: implications for melt evolution and the plumbing systems of monogenetic volcanoes. Earth Planet Sci Lett 269:478–487

Keiding JK, Trumbull RB, Veksler IV, Jerram DA (2011) On the significance of ultra-magnesian olivines in basaltic rocks. Geology 39(12):1095–1098

Larrea P, França Z, Lago M, Widom E, Galé C, Ubide T (2013) Magmatic processes and the role of antecrysts in the genesis of Corvo Island (Azores Archipelago, Portugal). J Petrol 54(4):769–793

Libourel G (1999) Systematics of calcium partitioning between olivine and silicate melt: implications for melt structure and calcium content of magmatic olivines. Contrib Miner Petrol 136(1–2):63–80

López-Escobar L, Cembrano J, Moreno H (1995) Geochemistry and tectonics of the Chilean Southern Andes basaltic Quaternary volcanism (37–46S). Andean Geol 22(2):219–234

Lupi M, Miller S (2014) Short-lived tectonic switch mechanism for long-term pulses of volcanic activity after mega-thrust earthquakes. Solid Earth 5(1):13

Maloney KT, Clarke GL, Klepeis KA, Quevedo L (2013) The Late Jurassic to present evolution of the Andean margin: drivers and the geological record. Tectonics 32:1049–1065

Mescua JF, Giambiagi LB, Tassara A, Gimenez M, Ramos VA (2014) Influence of pre-Andean history over Cenozoic foreland deformation: structural styles in the Malargüe fold-and-thrust belt at 35°S, Andes of Argentina. Geosphere 10(3):585–609

Morgado E, Parada MA, Contreras C, Castruccio A, Gutiérrez F, McGee LE (2015) Contrasting records from mantle to surface of Holocene lavas of two nearby arc volcanic complexes: Caburgua-Huelemolle Small Eruptive Centers and Villarrica Volcano, Southern Chile. J Volcanol Geoth Res 306:1–16

Muñoz J, Niemeyer H (1984) Hoja 64 Laguna del Maule, Regiones del Maule y Bio-Bio. Carta Geológica de Chile, Servicio Nacional de Geologıa y Mineria de Chile, scale, 1:250.000

Nakamura K (1977) Volcanoes as possible indicators of tectonic stress orientation—principle and proposal. J Volcanol Geoth Res 2(1):1–16

Németh K, Kereszturi G (2015) Monogenetic volcanism: personal views and discussion. Int J Earth Sci 104(8):2131–2146

Ozawa S, Nishimura T, Suito H, Kobayashi T, Tobita M, Imakiire T (2011) Coseismic and postseismic slip of the 2011 magnitude-9 Tohoku-Oki earthquake. Nature 475(7356):373–376

Piquer J, Castelli JC, Charrier R, Yáñez G (2010) El Cenozoico del alto río Teno, Cordillera Principal, Chile central: estratigrafía, plutonismo y su relación con estructuras profundas. Andean Geol 37(1):32–53

Piquer J, Skarmeta J, Cooke DR (2015) Structural evolution of the Rio Blanco-Los Bronces District, Andes of Central Chile: controls on stratigraphy, magmatism, and mineralization. Econ Geol 110(8):1995–2023

Ramos V (2009) Anatomy and global context of the Andes: main geologic features and the Andean orogenic cycle. Geol Soc Am Mem 204:31–65

Roberge J, Guilbaud MN, Mercer CN, Reyes-Luna PC (2015) Insight into monogenetic eruption processes at Pelagatos volcano, Sierra Chichinautzin, Mexico: a combined melt inclusion and physical volcanology study. Geol Soc Lond Spec Publ 410(1):179–198

Rodríguez C, Sellés D, Dungan M, Langmuir C, Leeman W (2007) Adakitic dacites formed by intracrustal crystal fractionation of water-rich parent magmas at Nevado de Longavi volcano (36.2° S; Andean Southern Volcanic Zone, Central Chile). J Petrol 48(11):2033–2061

Ruprecht P, Plank T (2013) Feeding andesitic eruptions with a high-speed connection from the mantle. Nature 500(7460):68–72

Ruprecht P, Bergantz GW, Cooper KM, Hildreth W (2012) The crustal magma storage system of Volcán Quizapu, Chile, and the effects of magma mixing on magma diversity. J Petrol 53(4):801–840

Salas P, Rabbia O, Ruprecht P, Bergantz G (2009) Geoquímica de los centros eruptivos menores y escoria máfica de la erupción de 1932 del volcán Quizapu, Región del Maule, Chile. XII Congreso Geológico Chileno, Santiago, S8_027, 1–3

Salas P, Rabbia OM, Hernández L (2014) High magnesium olivine in basaltic andesites from minor vents of Quizapu volcano, Southern Volcanic Zone, Chile. XIX Congreso Geológico Argentino, Córdoba S24:1–4

Salas P, Rabbia OM, Hernández L (2015) Compositional evolution of Los Hornitos mafic cones: insights from whole rock chemistry and high-resolution EMPA profiles in high-forsterite olivine phenocrysts. XIV Congreso Geológico Chileno, At1St3_026

Sellés D (2006) Stratigraphy, Petrology, and Geochemistry of Nevado de Longaví Volcano, Chilean Andes (36.2°S). Dissertation, University of Geneve

Sellés D, Rodriguez A, Dungan MA, Naranjo JA, Gardeweg M (2004) Geochemistry of Nevado de Longaví Volcano (36.2°S): a compositionally atypical arc volcano in the Southern Volcanic Zone of the Andes. Revista geológica de Chile 31(2):293–315

Singer B, Hildreth W, Vincze Y (2000) $^{40}Ar/^{39}Ar$ evidence for early deglaciation of the central Chilean Andes. Geophys Res Lett 27(11):1663–1666

Sisson TW, Grove TL (1993) Experimental investigations of the role of H_2O in calc-alkaline differentiation and subduction zone magmatism. Contrib Miner Petrol 113(2):143–166

Stern CR (2004) Active Andean volcanism: its geologic and tectonic setting. Revista geológica de Chile 31(2):161–206

Straub S, Gomez-Tuena A, Stuart F, Zellmer G, Espinasa-Perena R, Cai Y, Iizuka Y (2011) Formation of hybrid arc andesites beneath thick continental crust. Earth Planet Sci Lett 303(3):337–347

Takada Y, Fukushima Y (2013) Volcanic subsidence triggered by the 2011 Tohoku earthquake in Japan. Nat Geosci 6(8):637–641

Tassara A, Echaurren A (2012) Anatomy of the Andean subduction zone: three-dimensional density model upgraded and compared against global-scale models. Geophys J Int 189(1):161–168

Tormey D, Frey F, López-Escobar L (1995) Geochemistry of the active Azufre—Planchon—Peteroa volcanic complex, Chile (35° 15′ S): evidence for multiple sources and processes in a cordilleran arc magmatic system. J Petrol 36(2):265–298

Valentine GA, Gregg TKP (2008) Continental basaltic volcanoes-processes and problems. J Volcanol Geoth Res 177(4):857–873

Vergara M, Muñoz J (1982) La Formación Cola de Zorro en la alta cordillera andina chilena (36°–39° Lat. S), sus características petrográficas y petrológicas: una revisión. Andean Geol 17

Völker D, Kutterolf S, Wehrmann H (2011) Comparative mass balance of volcanic edifices at the southern volcanic zone of the Andes between 33°S and 46°S. J Volcanol Geoth Res 205(3):114–129

Weaver SL, Wallace PJ, Johnston AD (2011) A comparative study of continental vs. intraoceanic arc mantle melting: experimentally determined phase relations of hydrous primitive melts. Earth Planet Sci Lett 308(1):97–106

Wehrmann H, Hoernle K, Jacques G, Garbe-Schönberg D, Schumann K, Mahlke J, Lara LE (2014) Volatile (sulphur and chlorine), major, and trace element geochemistry of mafic to intermediate tephras from the Chilean Southern Volcanic Zone (33–43S). Int J Earth Sci 103(7):1945–1962

Wolff A (2005) Age and petrogenesis of lavas from the Casitas shield, Descabezado Grande-Cerro Azul volcanic complex, Chilean Andes. In: 2005 Salt Lake City annual meeting

Wolff A (2008) Chemical stratigraphy of lavas from the Casitas Shield, Descabezado Grande-cerro Azul volcanic complex, Chilean Andes. In: Goldschmidt conference